Full multiple-scattering calculations on silicates and oxides at the Al K edge

1996 J. Phys.: Condens. Matter 8 3691

(http://iopscience.iop.org/0953-8984/8/20/015)

J. Phys.: Condens. Matter **8** (1996) 3691–3704. Printed in the UK

Full multiple-scattering calculations on silicates and oxides at the Al K edge

Delphine Cabaret†, Philippe Sainctavit†‡, Philippe Ildefonse† and Anne-Marie Flank‡

† LMCP, URA 9, 4 place Jussieu, 75252 Paris Cédex 05, France
‡ LURE, Bâtiment 209d, Université Paris-Sud, 91405 Orsay, France

Received 3 January 1996, in final form 4 March 1996

Abstract. We present full multiple-scattering calculations at the aluminium K edge that we compare with experiments for four crystalline silicates and oxide minerals. In the different minerals aluminium atoms are either fourfold or sixfold coordinated to oxygen atoms in Al sites that are poorly symmetric. The calculations are based on different choices of one-electron potentials according to aluminium coordinations and crystallographic structures of the compounds. Hence it is possible to determine how the near-edge spectral features are a sensitive probe of the effective potential seen by the photoelectron in the molecular environment. The purpose of this work is to determine on the one hand the relation between Al K-edge spectral features and the geometrical arrangements around the aluminium sites, and on the other hand the electronic structure of the compounds.

1. Introduction

X-ray absorption spectroscopy in the vicinity of absorption edges contains information about the electronic structure and about the geometrical environment around the absorbing atom. Also, x-ray absorption near-edge structure (XANES) has been recognized as a valuable probe for studying the unoccupied electronic states in solids just above the Fermi level. Until recently, x-ray absorption of low-Z elements ($Z \leqslant 18$) in low-symmetry sites has not been widely addressed since it lies at the border of solid-state physics and atomic physics [1, 2, 3].

We have chosen to study the aluminium K edge for four minerals: corundum (α-Al_2O_3) and diaspore (α-AlOOH) where Al is coordinated to six oxygen atoms [4, 5], and berlinite ($AlPO_4$) and natrolite ($Na_2Al_2Si_3O_{10} \cdot 2H_2O$) where Al is coordinated to four oxygen atoms [6, 7]. In all of these compounds coordination polyhedra are characterized by distortions in Al–O distances and in O–Al–O bond angles. More details on the mineralogical interest of the present study are given in [8].

Al K-edge spectra have been recorded on the SA32 beam line of the French storage ring Super-ACO using two α-quartz ($10\bar{1}0$) monochromator crystals. The Super-ACO ring was operating at 800 MeV ($\lambda_c = 18.6$ Å) and 300 mA. A toroidal mirror in front of the beamline focused the beam to a dimension very close to that of the source: 200 μm horizontal and 500 μm vertical. The sample preparation consists in powder samples being mounted directly on copper slides after dispersion in acetone. The sample holder is transferred in the sample chamber where the pressure is below 10^{-5} hPa. Al K-edge spectra were collected over a photon energy range of 1550–1600 eV in 0.2 eV steps. The data were collected using

0953-8984/96/203691+14$19.50

entrance slits giving an energy resolution of about 0.5 eV. An aluminium metal foil (Al K edge: at 1559 eV [9, 10]) was used to ensure a consistent energy calibration for all the samples. Total electron yield detection was performed by recording total drain current.

X-ray absorption spectra have been calculated in the multiple-scattering formalism, with the 'extended Continuum' code developed by Natoli *et al* [11]. In this framework, the absorbing atom and surrounding atoms are modelled by a monoelectronic 'muffin-tin' potential. The potential is the central point in any multiple-scattering calculation. We have followed the potential construction as described by Levelut *et al* [12]. We have tested the convergence of the basis functions for the final state by calculating the total cross section at several test points for $3 \leqslant \ell_{max} \leqslant 5$ where ℓ_{max} is the maximum orbital angular momentum. It was found that for all calculations, the angular wave-function expansion could be truncated at $\ell_{max} = 3$. The first calculations were performed for large clusters, about 15 Å in diameter. Then the cluster size was decreased in order to examine the influence of medium-range order with respect to that of local order on the XANES spectral features. A scattering order analysis was also carried out to estimate the contribution of single scattering in the XANES region. The calculated spectra were convoluted with a Lorentzian function whose width at half-maximum is related to the effective mean free path of the photoelectron, which takes into account the experimental resolution (0.5 eV), the finite lifetime of the core hole (0.42 eV [13]) and the inelastic scattering of the photoelectron by the electrons of the materials.

The results are presented as follows. The sixfold-coordinated aluminium spectra are presented and interpreted in the second section. The third section is devoted to the fourfold-coordinated aluminium case, and the results are compared and discussed in the fourth section. The fifth section is a short conclusion.

Table 1. Al–O distances and O–Al–O bond angles in the first coordination sphere of corundum [4] and diaspore [5].

	Al–O distances		O–Al–O bond angles	
Corundum			$6\times O_1$–Al–O_2	86.4°
	$3\times$Al–O_1	1.97_0 Å	$3\times O_1$–Al–$O_{1'}$	79.7°
	$3\times$Al–O_2	1.86_0 Å	$3\times O_2$–Al–$O_{2'}$	101.1°
Diaspore			O_1–Al–O_2	97.6°
	Al–O_1	1.85_8 Å	O_2–Al–$O_{2'}$	100.4°
	$2\times$Al–O_2	1.85_1 Å	O_1–Al–O_4	91.0°
	Al–O_3	1.98_0 Å	O_2–Al–O_3	93.7°
	$2\times$Al–O_4	1.97_5 Å	O_2–Al–O_4	83.0°
			O_3–Al–O_4	92.2°

2. Sixfold-coordinated Al

The crystal structure of corundum, α-Al_2O_3, is trigonal and belongs to the trigonal Bravais lattice. There are two Al_2O_3 entities per rhombohedral unit cell (space group $R\bar{3}c$ or D^6_{3d}). The corundum structure can also be viewed as a hexagonal cell ($a_H = 4.7589$ Å, $c_H = 12.991$ Å) containing six Al_2O_3 units with alternate layers of Al and O atoms in planes perpendicular to the c-axis [4]. The unit cell of diaspore, α-AlOOH, has an orthorhombic structure with $a = 4.401$ Å, $b = 9.421$ Å, $c = 2.845$ Å, and contains four units of AlOOH. The space group is *Pbnm* (or D^{16}_{2h}). This crystal structure presents two kinds of

oxygen atom, one O ion and one OH group, and each aluminium atom has three oxygen atoms of each kind as neighbours [5]. In both compounds, aluminium atoms are sixfold coordinated to oxygen atoms and Al sites are weakly symmetric: the Al local point group is C_3 in corundum and C_s in diaspore. Table 1 summarizes the different Al–O distances and O–Al–O bond angles in the first coordination sphere of corundum and diaspore.

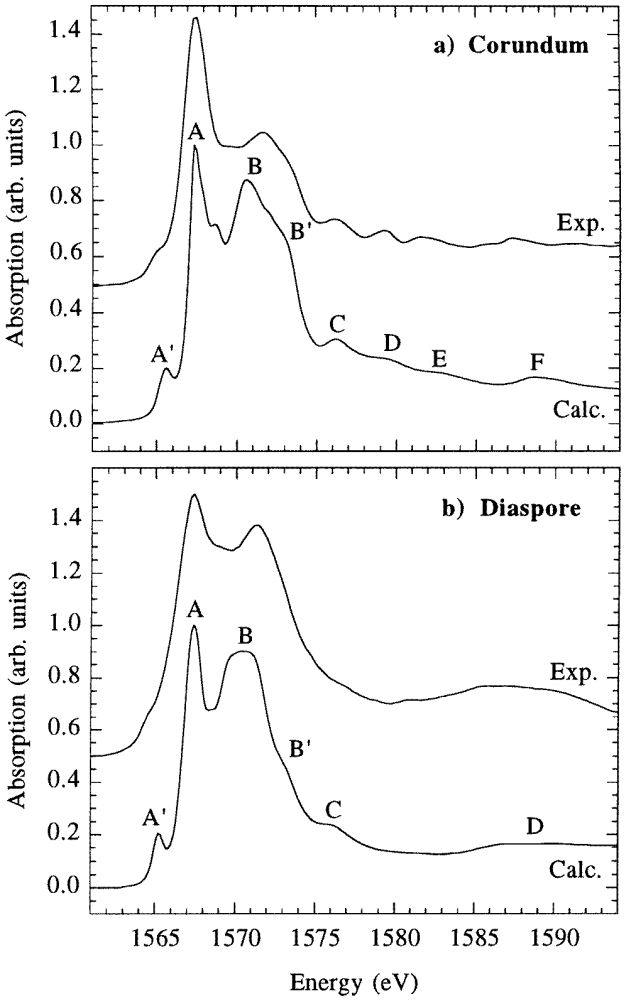

Figure 1. Experimental and calculated Al K-edge spectra of sixfold-coordinated Al compounds. (a) Corundum. (b) Diaspore.

The best agreement between experimental data and calculations was obtained with the Dirac–Hara exchange potential [14, 15], added to the Coulomb part of the potential. The Dirac–Hara exchange potential vanishes for high-energy photoelectrons [16]. It is less attractive than the X_α potential, so the features of the calculated spectra are not as much contracted as is usual with the X_α potential [17]. The potential of the excited state is supposed to be a relaxed and screened potential: we select the $Z+1$ atomic orbitals for the absorbing atom, i.e. atomic orbitals of silicon, remove a 1s electron (relaxation), and add an

extra electron on the outer orbital to mimic screening of the hole by the valence electrons. The consequent Al electronic configuration of the excited state is $1s^1 2s^2 2p^6 3s^2 3p^2$. In the calculations, we have sought to minimize the potential discontinuities at the surface of the muffin-tin spheres, since they represent a drawback of the simulation method. For this purpose, we have used a potential calculated with an overlap factor of 15% applied on the atomic spheres and chosen with the Norman prescriptions [18]; and we have reduced by 2.6 eV the interstitial potential calculated with the same overlap factor. Overlapping spheres have the advantage of reducing the interstitial region volume, where the poorest approximation to the potential is made [19].

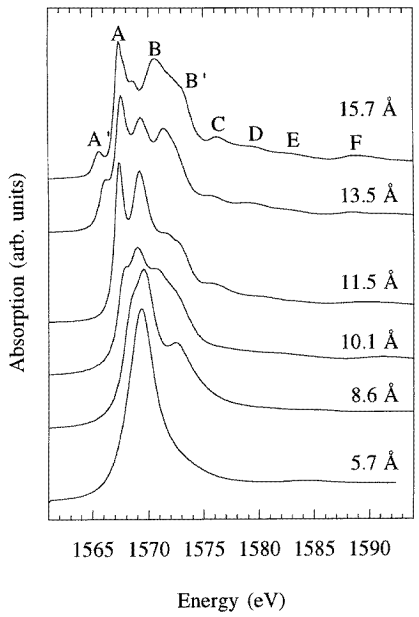

Figure 2. Calculated spectra of corundum for various cluster diameters (in Å).

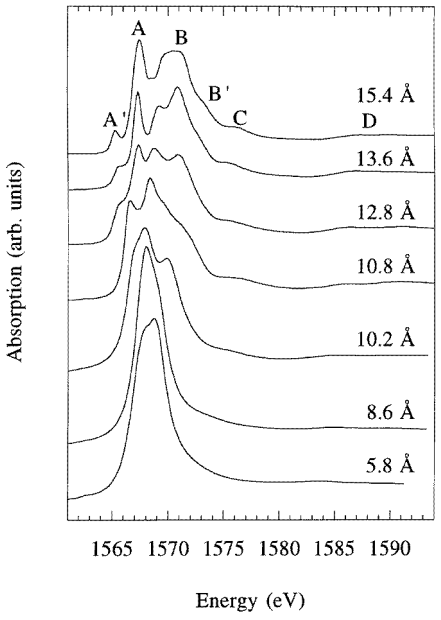

Figure 3. Calculated spectra of diaspore for various cluster diameters (in Å).

Figures 1(a) and 1(b) compare experimental and calculated spectra of corundum and diaspore, respectively. Firstly, one notices the fairly good agreement between calculations and experiment. Indeed all of the spectral features are reproduced by simulations: on the one hand, in the first 10 eV above the threshold, peak A′, the two main resonances A and B separated by a small plateau, and the shoulder B′; and on the other hand, in the energy range from 1575 to 1595 eV, the four well resolved features (C to F) of corundum and the two poorly resolved features (C at 1577 eV and the broad D at around 1590 eV) of diaspore.

In the energy range from 1566 to 1575 eV, the shape and the strength of the resonances strongly depend on the potential, and more precisely on the screening of the core hole. The feature A at 1567.4 eV corresponds in both cases to the main absorption peak and accounts for the Al 3p density of states. As regards the energy position of peaks B and B′, calculated spectra of corundum and diaspore exhibit the B resonance at 1570.5 eV while it arises at 1571.5 eV in the experimental spectra. In other words, A and B are more contracted in the theoretical spectra than in experimental spectra. We infer that the potential used for sixfold-coordinated aluminium compounds is too attractive. This can be explained at least in part

by the fact that the screening of the core hole taken into account here is too important. We will come back to this point in the fourth section.

Table 2. Cluster compositions.

Corundum		Diaspore	
Diameter (Å)	Composition	Diameter (Å)	Composition
5.7	1 Al 6 O	5.8	1 Al 3 O 3 OH
8.6	8 Al 12 O	8.6	9 Al 3 O 4 OH
10.1	15 Al 21 O	10.2	9 Al 9 O 11 OH
11.5	21 Al 36 O	10.8	11 Al 18 O 16 OH
		12.8	27 Al 24 O 25 OH
13.5	42 Al 51 O	13.6	35 Al 31 O 31 OH
15.7	59 Al 105 O	15.4	41 Al 48 O 45 OH

Berlinite		Natrolite	
Diameter (Å)	Composition	Diameter (Å)	Composition
4.9	1 Al 4 O	5.3	1 Al 4 O
8.9	1 Al 14 O 4 P	8.3	1 Al 4 O 4 Si 1 Na
		9.9	2 Al 8 O 4 Si 2 Na 2 H_2O
11.7	11 Al 32 O 8 P	11.0	2 Al 16 O 4 Si 3 Na 4 H_2O
13.6	15 Al 40 O 10 P	13.1	4 Al 26 O 8 Si 5 Na 6 H_2O
14.8	15 Al 62 O 14 P	14.7	6 Al 40 O 12 Si 9 Na 9 H_2O
		15.6	12 Al 50 O 14 Si 11 Na 9 H_2O

Calculations performed with various cluster sizes for corundum and diaspore are plotted in figures 2 and 3 respectively and their description is given in table 2. Firstly we notice that peak A′ is present only in spectra calculated with large clusters (more than 12 Å in diameter). It is therefore a signature of medium-range order. Thereby the present calculations are not in agreement with the results of Dien Li *et al* [2, 20], who assign peak A′ to the dipole-forbidden transition of Al 1s electrons to antibonding s-like states. In the present multiple-scattering framework the feature A′ is reproduced, while only transitions from 1s electrons towards the electric-dipole-allowed states (p states) are taken into account. Secondly, in the energy range from 1575 to 1595 eV, the features are also characterized by medium-range order. In the diaspore case, broad features C and D are clearly defined for a 10.8 Å diameter cluster. Likewise for corundum the 11.5 Å diameter cluster spectrum exhibits resonances C, D, E and F. Nevertheless these features are better resolved with a 13.5 Å diameter cluster. The spectra located at the bottom of figures 2 and 3 are calculated with a cluster composed by the absorbing atom and its six oxygen nearest neighbours (5.7 Å and 5.8 Å diameter clusters for corundum and diaspore respectively). Thus they illustrate the contribution of the coordination sphere to the spectra. This point will be discussed in the fourth section together with the spectra of the fourfold-coordinated aluminium.

We have also performed a scattering order analysis by calculating all possible scattering events attributed to one specific order. This calculates at one time the cross section attributed to all possible paths of a given scattering order. We made calculations from single scattering (EXAFS) to quadruple scattering. The nth-order scattering cross section is given by the following expression:

$$\sigma_n = \sigma_a \frac{-\kappa}{(2\ell+1)\sin^2\delta_\ell^0} \sum_{m=-\ell}^{\ell} \mathrm{Im}[(\kappa T_a H)^n T_a]^{0\ 0}_{\ell m \ell m}$$

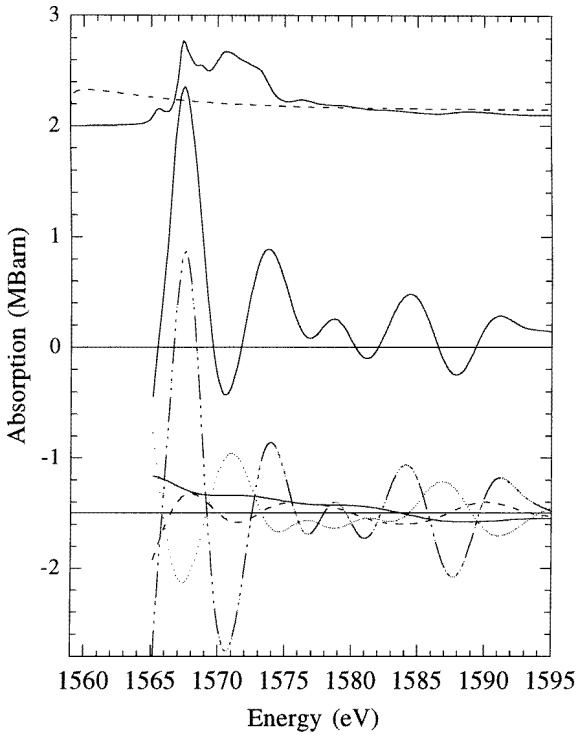

Figure 4. Scattering order analysis of corundum. Upper panel: the full multiple-scattering cross section ——, and the atomic cross section - - - -. Middle panel: the sum of the scattering series. Lower panel: the cross section for the nth-order scattering. σ_2: ——; σ_3: - - - -; σ_4: ·····; and σ_5: — · · — (see the text for more details).

where ℓ is the angular momentum of the final state, T_a is the atomic T-matrix, and H is the propagator. Our analysis provides evidence that neither single scattering nor the sum of scattering orders from single to fourth order could reproduce this feature. This is illustrated in figure 4 in the case of corundum where the full multiple-scattering cross section (upper panel) is compared with the sum of $\sigma_a + \sigma_2 + \sigma_3 + \sigma_4 + \sigma_5$ (middle panel). The lower panel of figure 4 plots the different σ_n for $2 \leqslant n \leqslant 5$. We calculated the eigenvalues of the operators $(\kappa T_a H)$ and found that around 10% of the eigenvalues are larger than 1 for large clusters (150 atoms). Then the absolute convergence of the series giving the equivalence between full multiple-scattering and scattering order analysis is not satisfied [21]. It is then not suprising that the scattering order series calculations do not converge towards full multiple-scattering spectra. We find the same conclusion for the resonances in the energy range 1564–1575 eV. In this energy range, very close to the edge, one knows that the resonances are caused by constructive interferences of many-order scattering processes. In the intermediate-energy range, this is less common and we attribute its origin to the small core-hole width that allows a large mean free path for the photoelectron. This effect implies calculations performed with large clusters for which the convergence of the scattering series is seldom met. In order to force the convergence of the scattering series associated with a 164-atom corundum cluster we performed a scattering order analysis with the imaginary part of the Hedin–Lundqvist potential to which we added an unrealistically

large core-hole width. Although the divergence is partially decreased in the edge region, the sum $\sigma_a + \sigma_2 + \sigma_3 + \sigma_4 + \sigma_5$ still remains very different from the full multiple-scattering calculation.

Table 3. Al–O distances and O–Al–O bond angles in the first coordination sphere of berlinite [6] and natrolite [7].

	Al–O distances		O–Al–O bond angles	
Berlinite			O_1–Al–O_2	109.2°
	2×Al–O_1	1.73_3 Å	O_1–Al–$O_{1'}$	112.1°
	2×Al–O_2	1.74_5 Å	O_1–Al–$O_{2'}$	107.1°
			O_2–Al–$O_{2'}$	112.3°
Natrolite			O_1–Al–O_2	108.2°
	Al–O_1	1.70_7 Å	O_1–Al–O_3	110.1°
	Al–O_2	1.71_1 Å	O_1–Al–O_4	112.0°
	Al–O_3	1.70_7 Å	O_2–Al–O_3	111.2°
	Al–O_4	1.71_0 Å	O_2–Al–O_4	105.3°
			O_3–Al–O_4	109.9°

3. Fourfold-coordinated Al

Berlinite, $AlPO_4$, consists of a three-dimensional alternation of slightly deformed AlO_4 and PO_4 tetrahedra which are corner linked by common oxygen atoms. The crystal symmetry is rhombohedral with a hexagonal Bravais lattice with $a = 4.943$ Å and $c = 10.948$ Å (space group $P3_121$ or D_3^4) and there are three $AlPO_4$ entities in the hexagonal cell. Berlinite, which is the isoelectronic compound of α-SiO_2, can be built up from quartz by alternately replacing the silicon atoms by phosphorus and aluminium atoms while simultaneously making small corrections to the bond lengths [6]. Natrolite crystallizes with orthorhombic symmetry ($a = 18.347$ Å, $b = 18.561$ Å, $c = 6.587$ Å) with eight $Na_2Al_2Si_3O_{10} \cdot 2H_2O$ formula units per unit cell (space group $Fdd2$ or C_{2v}^{19}). Its aluminosilicate framework is built up from interconnected chains of $(Si, Al)O_4$ tetrahedra along the crystal c-axis [7]. The aluminium site symmetry is C_2 for berlinite and C_1 for natrolite. The first-shell interatomic distances and bond angles are summarized in table 3.

The best agreement between experimental spectra and simulations was obtained with the Dirac–Hara potential, as in the sixfold-coordinated aluminium case. However, there is a large difference in the construction of the potential between sixfold- and fourfold-coordinated aluminium. In the case of fourfold-coordinated aluminium we started from a relaxed and unscreened potential. This means that the absorbing atom can relax under the core-hole attractive potential but there is no screening of the hole by the valence electrons. The starting potential can be described by a $1s^1 2s^2 2p^6 3s^2 3p^1$ configuration. We have made this choice after several tries and we shall discuss in section 4 the underlying physics that lies at the origin of this difference between fourfold and sixfold coordination for aluminium compounds.

Comparisons between calculations and experiment are shown in figure 5(a) for berlinite and figure 5(b) for natrolite. As explained above, the good agreement between calculations and experiment is due to the correct choice for the excited-state potential. Unlike the sixfold-coordinated Al case, the experimental spectra consist of a single well-identified resonance at 1566.4 eV for natrolite and at 1566.8 eV for berlinite. This A peak at the

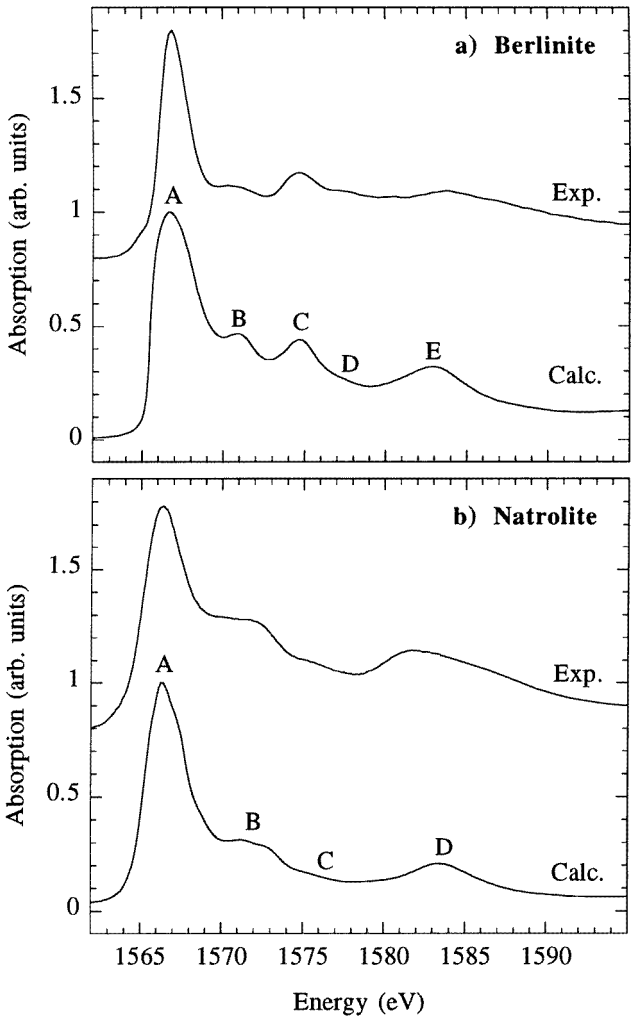

Figure 5. Experimental and calculated Al K-edge spectra of fourfold-coordinated Al compounds. (a) Berlinite. (b) Natrolite.

edge can be identified with a large p density of empty states localized on Al, very similar to an 'atomic' 3p level. In the pre-edge region of the berlinite spectrum, one notices the presence of a slight shoulder whose intensity is much fainter than that for the Al K edge in sixfold-coordinated Al compounds. In the case of the natrolite spectrum, the presence of such a feature is not obvious. For neither of the fourfold-coordinated compounds do the calculations clearly reproduce it, which is different to what happens for corundum and diaspore calculations. Thereby the origin of this feature might be different from that of peak A′ in sixfold-coordinated aluminium spectra. We do not want to be more precise since this energy region can be sensitive in the calculations to unphysical parameters like 'muffin-tin' radii. In the energy range from 1569 to 1595 eV, the simulations are close to the experiment: the four experimental structures of berlinite (B, C, D and E) and the three

resolved experimental features of natrolite (B, C and D) are well reproduced. The intensity of these structures depends on the cluster size.

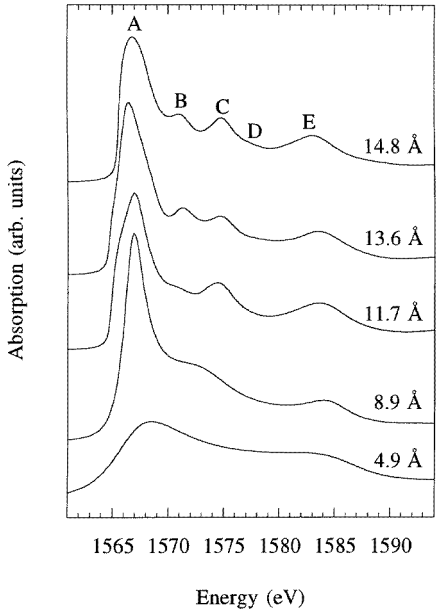

Figure 6. Calculated spectra of berlinite for various cluster diameters (in Å).

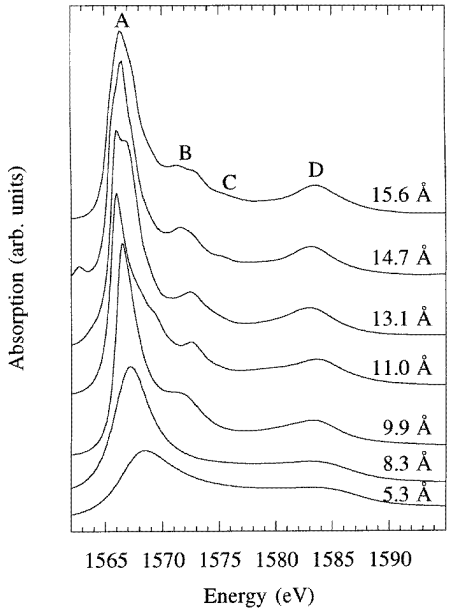

Figure 7. Calculated spectra of natrolite for various cluster diameters (in Å).

Figures 6 and 7 display calculated spectra with different cluster diameters for berlinite and natrolite respectively (see table 2 for information about the cluster size). Firstly, one notices the presence of peak E for berlinite and peak D for natrolite in the lowermost curves, which have been calculated with a cluster composed of the photoabsorber and its four nearest neighbours (4.4 Å and 5.2 Å diameter clusters for berlinite and natrolite respectively). Therefore the highest-energy feature in the fourfold-coordinated aluminium XANES spectra can be at least in part assigned to multiple scattering inside the first coordination sphere. This point will be discussed in the fourth section. Secondly, in the berlinite case, features B, C and D only appear for rather large clusters, and tend to become more intense with increasing cluster size: peak C at 1574.6 eV is well resolved with a 11.7 Å diameter cluster, peak B with a 13.6 Å diameter cluster, and shoulder D with a 14.8 Å diameter cluster. In the natrolite case, peak B arises in the spectrum calculated with a 9.9 Å diameter cluster, and peak D—although already present as a broad feature for the one-shell cluster—becomes well resolved for clusters larger than 13.1 Å in diameter. Resonance C, as in the case of resonance D for berlinite, is a shoulder and is only visible for the larger clusters. The two uppermost curves of figure 7 have virtually the same shape. Increasing the cluster size from 14.7 to 15.6 Å is essential to flatten the B resonance, leading then to a better match with experiment. In both fourfold-coordinated aluminium compounds, we find that the B structure is a relevant signature of medium-range order. We have also performed for berlinite and natrolite the same multiple-order analysis as in the case of sixfold-coordinated aluminium. We arrive at the same conclusion: XANES spectra of fourfold-coordinated aluminium compounds are strongly dominated by multiple scattering and medium-range order.

4. Discussion

From an experimental point of view, Al K-edge absorption spectroscopy is a very useful method for distinguishing tetrahedrally and octahedrally coordinated Al in crystalline and amorphous materials [3, 20, 22]. The experimental white line for fourfold-coordinated aluminium compounds is shifted towards lower energy by 0.6 to 1.0 eV as compared to the edge maximum of sixfold-coordinated aluminium XANES spectra. From our calculations we find that this shift can be related to a variation of the reference energies of the compounds studied. The reference energy, ϵ, is calculated as a function of the Coulomb part of the interstitial potential, $\tilde{V}_{cou}$, and of the interstitial electronic charge density, ρ: $\epsilon = \tilde{V}_{cou} + \hbar^2 k_F^2/2m + \tilde{V}_{ex}$ with $k_F^2 = (3\pi^2\rho)^{1/3}$ and where $\tilde{V}_{ex} = -3\alpha e^2 k_F/4\pi$ is the mean X_α exchange potential. We used the values of the α-parameter tabulated by Schwartz [23]. This ϵ-energy is the reference for the photoelectron momentum, k, defined by $E_i + \hbar\omega - \epsilon = \hbar^2 k^2/2m$, where E_i is the 1s binding energy and $\hbar\omega$ is the photon energy. Our calculations show that ϵ is lower for tetrahedral clusters than for octahedral clusters: the calculated ϵ-values of corundum and diaspore are -3.8 eV and -3.4 eV respectively while that for the natrolite is -4.8 eV and that for the berlinite is -4.2 eV (the zero of the calculation is the vacuum level). The difference between the ϵ-values has the same order of magnitude as the shift observed in the experimental spectra. From sections 2 and 3, we know that the final-state potential strongly depends on aluminium coordination: a screened potential has to be used for sixfold-coordinated Al while an unscreened core hole has to be considered for fourfold-coordinated Al. This strongly supports the assertion that the excited-state potential for fourfold-coordinated Al is more attractive—hence with ϵ more deeply buried below the vacuum level—than for sixfold-coordinated Al. This also compares well with information extracted from band-structure calculations and previous studies on the partial and local density of empty states of related compounds. To our knowledge, there are no calculated local and partial densities of states (DOS) available for berlinite. But since berlinite ($AlPO_4$) and quartz (SiO_2) are structurally similar and $AlPO_4$ is isoelectronic with SiO_2 [24], we have considered the electronic band structure of quartz [25, 26]. For sixfold-coordinated aluminium atoms we have selected the local and partial DOS of corundum [27, 28]. From the DOS calculations, one finds that the cation DOS close to the band gap is larger in corundum than in quartz. It is common to find that in tetrahedral oxide compounds the valence band maximum is almost always anion like with a strong p character. When the core hole is created, one expects the orbitals of the absorbing atom to be more strongly modified and the valence electrons close to the valence band maximum to be the most efficient in the screening of the core hole. If the cation density of states at the valence band is smaller in quartz than in corundum, one expects the core-hole screening to be less complete in quartz than in corundum. This fact can be related to strong resonance at the silicon K edge in quartz. The analogy between quartz and berlinite has certainly to be handled with care, but we think it sound as far as gross details such as cation core holes are concerned. From the understanding of the screening process, we can also understand the origin of a strong difference between fourfold- and sixfold-coordinated aluminium K edges. In the fourfold-coordinated aluminium K edge, the main feature close to the edge is a dominant peak whose width is around 4 eV. This fact can again be related to strong resonance at the silicon K edge in quartz. In the sixfold-coordinated aluminium K edge, the main rising edge is instead a 10 eV wide massif with two resonances. The more attractive the potential (the less screened the core hole), the more contracted is the density of empty states at the absorbing atom site.

Another interesting point concerns the relationship between the first coordination sphere

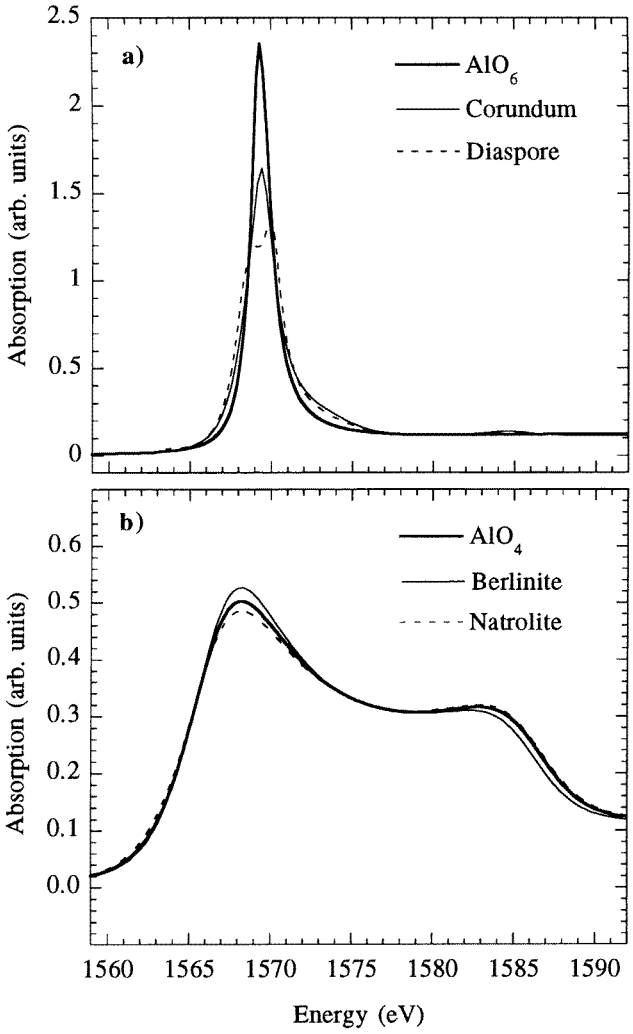

Figure 8. The influence of the first coordination sphere on calculated XANES spectra. (a) The sixfold-coordinated aluminium case: corundum and diaspore spectra are compared to the regular AlO_6 octahedron spectrum. (b) The fourfold-coordinated aluminium case: berlinite and natrolite spectra are compared to the regular AlO_4 tetrahedron spectrum.

and the calculated x-ray absorption spectrum that can be associated with it. XANES spectra calculated with a cluster composed of the photoabsorber and its nearest oxygen neighbours strongly depend on aluminium coordination. First of all, from the bottom spectra of figures 2, 3, 6 and 7 it is obvious that calculations performed with clusters containing only the coordination sphere completely fail to reproduce the features present in the experimental spectra. On the other hand, from previous calculations by other authors [1, 3, 29] one knows that the major scattering paths usually involve at least one of the atoms of the coordination sphere. It is then through such contributions that the atoms of the coordination sphere can play a role in the scattering process present in large clusters. It follows that the contribution

of the coordination sphere can be understood as a whole with the contributions of the more distant shells, and that it is very hazardous to try to extract experimental information when only scattering inside the coordination sphere is considered.

Although valuable information about the compound is hard to extract from coordination sphere calculations, the comparison of spectra calculated for the fourfold- or sixfold-coordinated cases can be fruitful. Figure 8(a) groups the sixfold-coordinated aluminium calculations: the coordination sphere cluster calculations (seven-atom cluster) are compared with the spectrum obtained for a regular oxygen octahedron with aluminium at its centre ($d_{Al-O} = 1.90$ Å, symmetry point group O_h or $m\bar{3}m$). The three spectra are characterized by only one resonance at 1569.3 eV, whose strength and width can be related to octahedron distortions: its intensity decreases and its width increases as distortions from the perfect octahedron become more important. Table 1 does show that diaspore displays a larger range of Al–O distances and O–Al–O bond angles inside the first coordination sphere than in corundum. Furthermore for diaspore the absorption peak exhibits a small bump on its low-energy side at 1568.9 eV. The presence of this shoulder reflects the fact that the diaspore octahedron is more distorted than the corundum one [29]. In figure 8(b) the fourfold-coordinated aluminium case is plotted: calculations with a five-atom cluster for berlinite and natrolite are compared with a calculated spectrum for a regular oxygen tetrahedron with aluminium at the centre ($d_{Al-O} = 1.72$ Å, symmetry point group T_d or $4\bar{3}m$). The three spectra are almost identical: they exhibit two features, one corresponding to the same energy as the white line (around 1568 eV) and another one at higher energy (around 1583 eV) that corresponds to peak E for berlinite and peak D of natrolite. The distortions of the tetrahedra do not affect the total cross section, unlike in the sixfold-coordinated aluminium case. Finally it is important to notice a fundamental difference between the spectra for tetrahedron and octahedron calculations: octahedron calculations produce only one peak, while tetrahedron ones produce two features. The broad resonance present in both the berlinite and the natrolite K edge certainly originates partly from the coordination sphere symmetry. From figures 6 and 7, one sees that the resonance is also substantially determined by the more distant neighbouring shells, and the contribution of the whole cluster finally determines the exact energy and intensity of the resonance. This very local origin for this feature is fully supported by the examination of many aluminium K-edge spectra in tetrahedral coordination.

5. Conclusion

Multiple-scattering calculations at the aluminium K edge have been compared with Al K-edge XANES spectra of silicates and oxide minerals. Thanks to this powerful theoretical method, most of x-ray absorption spectral features can be interpreted.

Firstly, we have shown that full multiple-scattering calculations provide important information about the electronic structure of the compounds. Indeed the potential used in the simulations strongly depends on the aluminium site symmetry and on the aluminium coordination number. According to the local environment of the photoabsorber (sixfold or fourfold coordinated to oxygen atoms), a screening of the core hole can be necessary, in order to yield a good agreement in the first 10 eV of the spectra.

Secondly, calculations have revealed that decreasing the cluster size dramatically modifies the spectral features. Except resonances E (berlinite) and D (natrolite), present in spectra calculated with a five-atom cluster, all of the features located above the absorption peak are related to medium-range order. First-coordination-sphere calculations for sixfold-coordinated Al minerals are basically different from those corresponding to fourfold-

coordinated Al compounds, and both calculations yield spectra that are obviously very different from the experimental results. This indicates that large-cluster calculations are essential to mimic the spectra, at least in the very-near-edge region, i.e. for the first 15 eV above the main rising edge. In this energy range, the photoelectron kinetic energy is not large enough to interact inelastically with the plasmons, and the photoelectron mean free path is only limited by the aluminium 1s core-hole lifetime. From our calculations and work by others [30], the photoelectron mean free path can be larger than 30 Å. This remark is mainly valid for very near the edge for the aluminium K edge.

Thirdly, evidence has been provided to show that single scattering and higher-order scattering are not valuable for reproducing aluminium K-edge spectral features in the near-edge region. Although path analysis, as developed by several authors [31, 32], proved to be an effective method in numerous XAFS studies [33, 34], full multiple-scattering calculations are certainly to be preferred for XANES of low-Z-element K edges.

Acknowledgments

This work was partly supported by the EU Human Capital and Mobility Network, No ERBCHXCT930360. We are grateful to Christian Brouder for enlightening conversations and to Valérie Briois for making possible part of the calculations.

References

[1] Chaboy J, Benfatto M and Davoli I 1995 *Phys. Rev.* B **52** 10 014
[2] Li Dien, Bancroft G M, Fleet M E, Feng X H and Pan Y 1995 *Am. Mineral.* **80** 432
[3] McKeown D A 1989 *Phys. Chem. Minerals* **16** 678
[4] Newnham R E and de Haan Y M 1962 *Z. Kristallogr.* **117** 235
[5] Busing W R and Levy H A 1958 *Acta Crystallogr.* **11** 798
[6] von Schwarzenbach D 1966 *Z. Kristallogr.* **123** 161
[7] Alberti A, Cruciani G and Dauru' I 1995 *Eur. J. Mineral.* **7** 501
[8] Ildefonse P, Cabaret D, Sainctavit P, Flank A-M and Lagarde P 1996 *Phys. Chem. Minerals* submitted
[9] Ildefonse P, Kirkpatrick R J, Montez B, Calas G, Flank A-M and Lagarde P 1994 *Clays Clay Minerals* **42** 276
[10] Wong J, George G N, Pickering I J, Zek Z U, Rowen M, Tanaka T, Via G H, De Vries B, Vaughan D E W and Brown G E 1994 *Solid State Commun.* **92** 559
[11] Natoli C R, Misemer D K, Doniach S and Kutzler F W 1980 *Phys. Rev.* A **22** 1104
[12] Levelut C, Sainctavit P, Ramos A and Petiau J 1995 *J. Phys.: Condens. Matter* **7** 2353
[13] Krause M O and Olivier J H 1979 *J. Phys. Chem. Ref. Data* **8** 329
[14] Dirac P M 1930 *Proc. Cambridge Phil. Soc.* **26** 376
[15] Hara S 1967 *J. Phys. Soc. Japan* **22** 710
[16] Chou S-H, Rehr J J, Stern E A and Davidson E R 1987 *Phys. Rev.* B **35** 2604
[17] Sainctavit P 1989 *PhD Thesis* Université Paris 7
[18] Norman J G Jr 1976 *Mol. Phys.* **31** 1191
[19] Kutzler F V, Natoli C R, Misemer D K, Doniach S and Hodgson K O 1980 *J. Chem. Phys.* **73** 3274
[20] Li Dien, Bancroft G M, Fleet M E and Feng X H 1995 *Phys. Chem. Minerals* **22** 115
[21] Natoli C R and Benfatto M 1986 *J. Physique Coll.* **47** C8 11
[22] Ildefonse P, Calas G, Flank A-M and Lagarde P 1995 *Nucl. Instrum. Methods. Phys. Res.* B **97** 172
[23] Schwartz K 1972 *Phys. Rev.* B **5** 2466
[24] Schober H and Dorner B 1994 *J. Phys.: Condens. Matter* **6** 5351
[25] Jollet F and Noguera C 1993 *Phys. Status Solidi* b **179** 473
[26] Xu Y-N and Ching W Y 1991 *Phys. Rev.* B **44** 11 048
[27] Kefi M, Jonnard P, Vergand F, Bonnelle C and Gillet E 1993 *J. Phys.: Condens. Matter* **5** 8629
[28] Ching W Y and Xu Y-N 1994 *J. Am. Ceram. Soc.* **77** 404
[29] Paris E and Tyson T A 1994 *Phys. Chem. Minerals* **21** 299
[30] Zabinsky S I 1993 *PhD Thesis* University of Washington

[31] Rehr J J and Albers R C 1990 *Phys. Rev.* B **41** 8139
[32] Filipponi A, Di Cicco A, Tyson T A and Natoli C R 1991 *Solid State Commun.* **78** 265
[33] Rehr J J, Albers R C and Zabinsky S I 1992 *Phys. Rev. Lett.* **69** 3397
[34] Le Fèvre P, Magnan H, Heckmann O and Chandesris D 1995 *Physica* B **208+209** 401